Buckling of porous FGM beams considering the thickness stretching effect

Ahmed Amine Daikh[1,2*], Mohamed Ouedjdi Belarbi[3],
Mohamed Sid Ahmed Houari[2], Mohamed A. Eltaher[4,5]

[1]University Center of Naama, Naama, Algeria
[2]Université Mustapha Stambouli, Mascara, Algerie
[3]Université de Biskra, Biskra, Algeria
[4]King Abdulaziz University, Jeddah, Saudi Arabia
[5]Zagazig University, Zagazig, Egypt
[*]Corresponding author: daikhresearch@gmail.com

ARTICLE INFO	ABSTRACT

This study presents a novel analytical investigation into the buckling behavior of porous Functionally Graded (FG) beams, incorporating the effects of thickness stretching and porosity variations. Unlike conventional approaches that assume porosity is purely governed by the rule of mixtures, this work introduces a novel perspective by directly relating porosity to the material volume fraction. Two distinct porosity schemes are analyzed: Volume Fraction-Dependent porosity (VFD) and Rule of Mixtures-Dependent porosity (RMD), with four porosity distribution types - Even, Uneven, Linear (1), and Linear (2). A higher-order shear deformation theory is developed to account for the thickness stretching effect, enabling precise modeling of transverse shear stresses without the need for correction factors. The equilibrium equations are derived using the principle of virtual work and solved via the Galerkin method for a range of boundary conditions. Comprehensive parametric studies reveal the influence of structural geometry, material grading, and porosity types on the critical buckling loads. The findings demonstrate the robustness of the proposed framework and offer new insights for designing lightweight and efficient FG structures.

1. Introduction

Functionally Graded Structures (FGS) are advanced materials characterized by a continuous variation in composition and properties, allowing for tailored mechanical performance in various applications. The incorporation of porosity in FGS offers significant advantages, such as reduced weight, improved thermal insulation, and enhanced energy absorption capabilities, making them suitable for lightweight applications in aerospace and automotive industries. However, the presence of porosity can also lead to disadvantages, including decreased mechanical strength and stiffness, which may compromise structural integrity under certain loading conditions. Consequently, the design of functionally graded structures with porosity requires careful optimization to balance these benefits and drawbacks. Understanding the interplay between porosity and material properties is crucial for maximizing performance while ensuring reliability.

Numerous studies have investigated the effects of porosity on the mechanical behavior of Functionally Graded (FG) beams. To investigate the nonlinear static deflections of functionally graded materials with porosity under thermal effects, Akbaş (2017) employed a comprehensive Lagrangian finite element method within a two-dimensional continuum framework, utilizing the

Newton - Raphson approach. Atmane et al. (2017) accounted for the effects of thickness stretching and porosity in their vibrational analysis of functionally graded beams. Su et al. (2019) examined the impact of surface effects on the static bending behavior of porous functionally graded nanobeams subjected to a concentrated transverse load, applying Reddy's higher-order beam theory. Following Timoshenko beam theory, Mojahedin et al. (2018) conducted a thermoelastic analysis of functionally graded porous beams under in-plane thermal loading, which was applied uniformly across the entire beam. Burlayenko and Kouhia (2024) explored the free vibration characteristics of Functionally Graded Beams (FGBs) with various rectangular cross-sectional shapes and four distinct porosity distribution patterns, employing the Differential Transform Method (DTM) while validating their results with a beam model solution to the motion equation. Eltaher et al. (2018) examined the mechanical bending and vibrational behavior of functionally graded porous nanobeams through the application of Euler - Bernoulli theory and Finite Element Methods (FEM). Zouatnia et al. (2024) analyzed the natural oscillations of bi-directional functionally graded beams using Reddy's Shear Deformation Theory (RSDT) and Navier's method, focusing on composite materials comprising metal and ceramic components. They calculated the elasticity modulus and density to evaluate how grading parameters influence the natural frequency by analyzing their effects in both the thickness and longitudinal directions. Utilizing Reddy's third-order shear deformation theory along with the nonlinear von-Kármán strain-displacement relationship, Srikarun et al. (2021) examined both linear and nonlinear bending behaviors of functionally graded porous beams. Hamed et al. (2019) applied Euler - Bernoulli beam theory and finite element methods to model the mechanical bending characteristics of functionally graded porous nanobeams. Sah and Ghosh (2022) explored how multi-directional porosity distributions affect the free vibration and buckling of porous functionally graded plates, proposing an analytical solution based on Navier's method. Bagheri et al. (2024) investigated the influence of pores on the natural frequency and buckling behavior of beams using Classical Beam Theory (CBT) and the Differential Quadrature Method (DQM). Additionally, Fahsi et al. (2019) employed a novel enhanced quasi-3D shear deformation theory and Navier's solution to study the bending, buckling, and free vibration responses of functionally graded porous beams supported by an elastic foundation. A finite element model grounded in first-order shear deformation theory was employed by Zghal and Dammak (2021) to analyze the buckling responses of porous structural components subjected to various compressive loads. Beitollahi et al. (2024) explored the free vibration and static bending behaviors of both porous and non-porous square microplates and nanoplates, discovering that a variable length scale parameter increased the stiffness and stability of the plates using the Modified Couple Stress Theory (MCST). Utilizing a trigonometric shear deformation theory in conjunction with finite element methods, Zhang et al. (2020) examined the damping and free vibration properties of porous functionally graded sandwich plates through the modified Fourier - Ritz method, integrated with first-order shear deformation theory, analyzing the effects of both even and uneven porosities on natural vibration and damping performance. Polit et al. (2019) employed Navier's solutions alongside a higher-order shear deformation theory to study the static bending and elastic stability of thick functionally graded graphene platelets reinforced porous nanocomposite curved beams. Lastly, Adhikari et al. (2020) proposed a finite element model based on higher-order shear deformation theory to conduct buckling analysis of porous sandwich functionally graded material plates under various compressive loads.

Masjedi et al. (2019) employed an orthogonal Chebyshev collocation method to analyze the large deflection behavior of functionally graded porous beams subjected to both conservative and non-conservative loading conditions. Wang et al. (2020) developed a high-order shear deformable beam model to investigate the transient response of Porous Sandwich Beams (PSBs). Gao and Xiao (2019) studied the nonlinear bending behavior of functionally graded porous nanobeams under various physical stresses using a two-step perturbation technique alongside nonlocal strain gradient theory. Wattanasakulpong and Ungbhakorn (2014) examined the

nonlinear vibrational responses of functionally graded porous beams with restrained ends. Liu et al. (2019) investigated the coupling of thermal and mechanical buckling phenomena in a clamped functionally graded sandwich beam by utilizing high-order sinusoidal shear deformation theory. Additionally, a quasi-3D shear deformation theory was applied to assess the vibrational characteristics of functionally graded porous plates (Mellal et al., 2021) supported by a Winkler-Pasternak foundation. This approach effectively reduced the number of unknown variables while evaluating the impacts of factors such as porosity, volume fraction index, thickness ratio, and wave number. Using a modified mixed finite element beam model, Zghal et al. (2020) examined the impact of porosity on the static bending behavior of functionally graded beams. Fallah and Aghdam (2024) applied physics-based neural networks to investigate the bending and vibrational responses of functionally graded porous beams. They utilized Hamilton's principle to derive the equations of motion and trained the network parameters to explore how factors such as porosity, material distribution, porosity distribution type, and elastic foundation influence structural behavior. Hamed et al. (2020) proposed a parabolic higher-order shear deformation model to optimize critical buckling loads for thin and thick functionally graded sandwich beams with porous cores. In another study, Zhang et al. (2024) employed Timoshenko beam theory, Modified Couple Stress Theory (MCST), and the von Kármán geometric nonlinearity hypothesis to evaluate various factors affecting vibrational behavior, including platelet distribution, taper ratio, and boundary conditions. Finally, the nonlinear vibration of shear deformable porous sandwich beams was presented in reference (Chen et al., 2016), utilizing Timoshenko beam theory.

This paper explores the buckling behavior of Functionally Graded (FG) plates by relating porosity to the volume fraction, diverging from previous research that typically associates porosity with the rule of mixtures. The analysis is based on higher-order shear deformation theory, and the equilibrium equations are solved using Galerkin's method.

2. Material properties

Consider an FG beam with length and thickness "L×h" (Figure 1). Poisson's ratio ν v is assumed to be constant. In this study, two scenarios regarding material constituents dependent on porosity are examined: dependence on the volume fraction of porosity (VFD) and dependence on the porosity mixing rule (RMD). The effective mechanical properties and volume fraction of Functionally Graded Materials (FGM) that account for the influence of porosity can be defined as follows:

2.1. Volume Fraction Porosity Dependent (VFD)

The volume fraction of the ceramic phase, including the effect of porosity, can be expressed as follows:

$$V(z) = \left(\frac{1}{2} + \frac{z}{h}\right)^p - \Theta(z) \tag{1}$$

Where p and $\Theta(z)$ is the power law index and the porosity distribution function, respectively. The Young's modulus "E" can be expressed as functions of the material composition or other relevant parameters.

$$E(z) = (E_c - E_m)V_c + E_m \tag{2}$$

Where the subscripts "m" and "c" denote the metallic and ceramic constituents, respectively, and "V_c" represents the volume fraction of the ceramic phase within the beam.

2.2. Rule Mixture Porosity Dependent (RMD)

In the case of porosity dependence based on the mixing rule, the volume fraction of the ceramic phase in the x-direction can be calculated as follows:

$$V(z) = \left(\frac{1}{2} + \frac{z}{h}\right)^p \tag{3}$$

Where material properties according to the the rule of mixture is given by:

$$E(z) = E_m + (E_c - E_m)V_c - \Theta(z) \tag{4}$$

Four types of porosity distributions have been investigated: even distribution, uneven distribution, linear distribution (1), and linear distribution (2). The function that characterizes the porosity can be expressed as follows:

Even porosity:

$$\Theta(z) = \frac{\xi}{2} \tag{5}$$

Uneven porosity:

$$\Theta(z) = \frac{\xi}{2}\left(1 - \frac{2|z|}{h}\right) \tag{6}$$

Linear (1) porosity:

$$\Theta(z) = \frac{\xi}{2}\left(\frac{1}{2} + \frac{z}{h}\right) \tag{7}$$

Linear (2) porosity:

$$\Theta(z) = \frac{\xi}{2}\left(\frac{2z-1}{2h}\right) \tag{8}$$

The porosity coefficient is defined by the symbol ξ, where $0 \le \xi \le 0.2$. A comparison analysis between the effect of the first porosity scheme "VFD" and the other "RMD" on the Young's modulus of the FGM plate is plotted in **Figure 2**, considering the different types of porosity. It is clear that "RMD" has a greater influence on the elastic modulus compared to "VFD".

The porosity coefficient is represented by the symbol ξ, where $0 \le \xi \le 0.2$. A comparative analysis of the effects of the first porosity scheme, "VFD," and the alternative scheme, "RMD," on the Young's modulus of the FGM plate is illustrated in Figure 2, taking into account the various types of porosity. The results indicate that "RMD" has a more significant impact on the elastic modulus than "VFD".

Figure 1

Geometry of The FG Beam
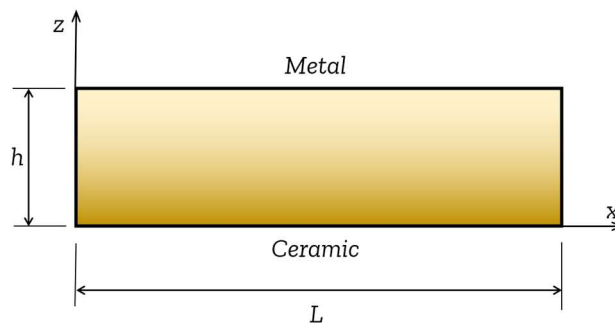
Source. The researcher's data analysis

Figure 2

Influence of The Porosity Scheme on Young's Modulus (p = 2, ξ = 0.2)
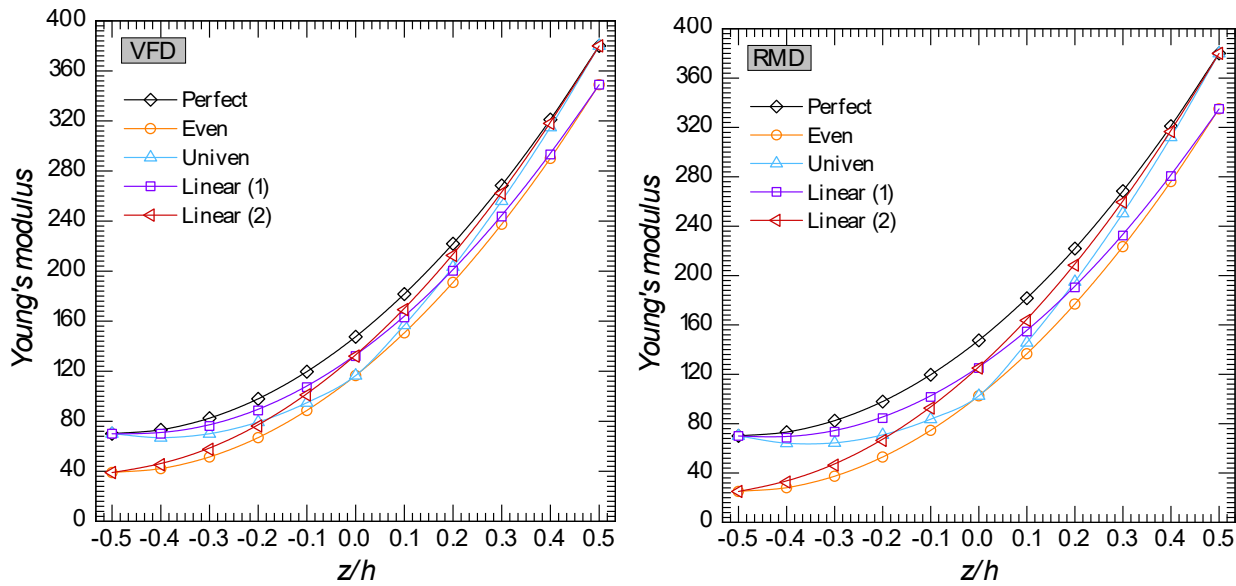
Source. The researcher's data analysis

3. Displacement field

The equilibrium equations governing the bending response of Functionally Graded Material (FGM) beams are established using a quasi-3D shear deformation theory. The total displacement at any point within the structure can be represented as follows:

$$u(x, z, t) = u_0 - z \frac{\partial w_0}{\partial x} + \Phi(z)\varphi_x$$
$$w(x, z, t) = w_0 + \Phi(z)'\varphi_z \tag{9}$$

The shape function $\Phi(z)$, which defines the distribution of transverse shear strains and stresses through the thickness of the nanobeam, is expressed as follows:

$$\Phi(z) = 5h \times \mathrm{atan}\left(\frac{z}{h}\right) - 4z \tag{10}$$

The shape function $\Phi(z)$ is selected to ensure compliance with the stress-free boundary conditions at both the top and bottom surfaces of the nanobeam, thereby eliminating the need for a shear correction factor.

The nonzero strains corresponding to the deformations described above are given by:

$$\begin{Bmatrix} \sigma_{xx} \\ \sigma_{zz} \\ \tau_{xz} \end{Bmatrix} = \begin{bmatrix} Q_{11} & Q_{13} & 0 \\ Q_{13} & Q_{33} & 0 \\ 0 & 0 & Q_{55} \end{bmatrix} \begin{Bmatrix} \varepsilon_{xx} \\ \varepsilon_{zz} \\ \gamma_{xz} \end{Bmatrix} \tag{11}$$

Since the normal strain in the z-direction can be neglected (indicating non-stretching), we have $\varepsilon_{zz}^{(0)} = 0$. Therefore, it follows that:

$$Q_{11} = \frac{E}{1 - v^2}$$
$$Q_{13} = \frac{vE}{1 - v}$$
$$Q_{55} = \frac{E}{2(1 + v)} \tag{12}$$

4. Variational statements

The total potential energy principle is utilized to derive the equilibrium equations for the

FG nanobeams:

$$\int_{-h/2}^{h/2}\int_0^L [\sigma_{xx}\delta\varepsilon_{xx} + \sigma_{zz}\varepsilon_{zz} + \tau_{xz}\gamma_{xz}]\,dxdz - \int_0^L N_x^0 \frac{\partial w_0}{\partial x}\frac{\partial \delta w_0}{\partial x}\,dx$$
$$- \int_0^L k_w w_0 \delta w_0 + k_g \frac{\partial w_0}{\partial x}\frac{\partial \delta w_0}{\partial x} + k_w w_0^3 \delta w_0 dx \tag{13}$$

k_w and k_g represent the linear Winkler stiffness and the shear layer stiffness, respectively. The equilibrium equations can be expressed as follows:

$$\frac{\partial N_{xx}}{\partial x} = 0$$
$$\frac{\partial^2 M_{xx}}{\partial x^2} - N_x^0 \frac{\partial^2 w_0}{\partial x^2} - k_w w_0 + k_g \frac{\partial^2 w_0}{\partial x^2} - k_{NL}w_0^3 = 0$$
$$\frac{\partial P_{xx}}{\partial x} - Q_{xz} = 0 \tag{14}$$
$$\frac{\partial Q_{xz}}{\partial x} - R_z = 0$$

Where

$$N_{xx} = \int_{-h/2}^{h/2}\sigma_{xx}\,dz = A_{11}\frac{\partial u_0}{\partial x} - B_{11}\frac{\partial^2 w_0}{\partial x^2} + C_{11}\frac{\partial \varphi_x}{\partial x} + A_{13}\varphi_z$$

$$M_{xx} = \int_{-h/2}^{h/2}\sigma_{xx}z\,dz = B_{11}\frac{\partial u_0}{\partial x} - D_{11}\frac{\partial^2 w_0}{\partial x^2} + F_{11}\frac{\partial \varphi_x}{\partial x} + B_{13}\frac{\partial \varphi_z}{\partial x}$$

$$P_{xx} = \int_{-h/2}^{h/2}\sigma_{xx}\Phi(z)\,dz = C_{11}\frac{\partial u_0}{\partial x} - F_{11}\frac{\partial^2 w_0}{\partial x^2} + H_{11}\frac{\partial \varphi_x}{\partial x} + C_{13}\varphi_z \tag{15}$$

$$Q_{xz} = \int_{-h/2}^{h/2}\tau_{xz}\Phi(z)'\,dz = A_{55}\left(\varphi_x + \frac{\partial \varphi_z}{\partial x}\right)$$

$$R_z = \int_{-h/2}^{h/2}\sigma_{zz}\Phi(z)''\,dz = A_{13}\frac{\partial u_0}{\partial x} - B_{13}\frac{\partial^2 w_0}{\partial x^2} + C_{13}\frac{\partial \varphi_x}{\partial x} + D_{13}\varphi_z$$

5. Nonlocal strain gradient theory

By considering the combined physical effects of strain gradient stress and nonlocal elastic stress fields, a stress function is proposed as follows:

$$\sigma_{ij} = \sigma_{ij}^{(0)} - \frac{d\sigma_{ij}^{(1)}}{dx} \tag{16}$$

Where $\sigma\sigma_{ij}^{(0)}$ and $\sigma_{ij}^{(1)}$ represent the classical stress corresponding to the strain ε_{kl} and the higher-order stress $\sigma_{ij}^{(1)}$ corresponding to the strain gradient $\varepsilon_{kl,x}$, respectively. These can be expressed as:

$$\sigma_{ij}^{(0)} = \int_0^L C_{ijkl}\alpha_0(x,x',e_0a)\varepsilon_{kl,x}(x')dx'$$
$$\sigma_{ij}^{(1)} = l^2\int_0^L C_{ijkl}\alpha_1(x,x',e_1a)\varepsilon_{kl,x}(x')dx' \tag{17}$$

C_{ijkl} denotes an elastic constant, and l l is the material length scale parameter introduced to account for the influence of the strain gradient stress field. The parameters ee_0a and e_1a are nonlocal parameters introduced to capture the significance of the nonlocal elastic stress field.

The nonlocal kernel functions $\alpha_0(x,x',e_0a)$ and $\alpha_1(x,x',e_1a)$ satisfy the established conditions. Consequently, the general constitutive relation can be expressed as:

$$[1 - (e_1a)^2\nabla^2][1 - (e_0a)^2\nabla^2]\sigma_{ij} = C_{ijkl}[1 - (e_1a)^2\nabla^2]\varepsilon_{kl} - C_{ijkl}l^2[1 - (e_0a)^2\nabla^2]\nabla^2\varepsilon_{kl} \tag{18}$$

∇^2 denotes the Laplacian operator. In the current analysis, we assume that the coefficient $e = e_0 = e_1$. Therefore, the total nonlocal strain gradient constitutive relation can be expressed as

$$[1 - \mu\nabla^2]\sigma_{ij} = C_{ijkl}[1 - \lambda\nabla^2]\varepsilon_{kl} \tag{19}$$

Where $\mu = (ea)^2$ and $\lambda = l^2$.

Based on the nonlocal strain gradient theory, the equilibrium equations can be formulated as:

$$\left(1 - \lambda \frac{\partial^2}{\partial x^2}\right)\left(A_{11}\frac{\partial^2 u_0}{\partial x^2} - B_{11}\frac{\partial^3 w_0}{\partial x^3} + C_{11}\frac{\partial^2 \varphi_x}{\partial x^2} + A_{13}\frac{\partial \varphi_z}{\partial x}\right) = 0$$

$$\left(1 - \lambda \frac{\partial^2}{\partial x^2}\right)\left(B_{11}\frac{\partial^3 u_0}{\partial x^3} - D_{11}\frac{\partial^4 w_0}{\partial x^4} + F_{11}\frac{\partial^3 \varphi_x}{\partial x^3} + B_{13}\frac{\partial^2 \varphi_z}{\partial x^2}\right)$$

$$-\left(1 - \mu \frac{\partial^2}{\partial x^2}\right)\left(N_x^0 \frac{\partial^2 w_0}{\partial x^2} - k_w w_0 - k_g \frac{\partial^2 w_0}{\partial x^2} - k_w w_0{}^3\right) = 0 \qquad (20)$$

$$\left(1 - \lambda \frac{\partial^2}{\partial x^2}\right)\left(C_{11}\frac{\partial^2 u_0}{\partial x^2} - F_{11}\frac{\partial^3 w_0}{\partial x^3} + H_{11}\frac{\partial^2 \varphi_x}{\partial x^2} A_{55}\varphi_x - (A_{55} - C_{13})\frac{\partial \varphi_z}{\partial x}\right) = 0$$

$$\left(1 - \lambda \frac{\partial^2}{\partial x^2}\right)\left(-A_{13}\frac{\partial u_0}{\partial x} + B_{13}\frac{\partial^2 w_0}{\partial x^2} + (A_{55} - C_{13})\frac{\partial \varphi_x}{\partial x} + A_{55}\frac{\partial^2 \varphi_z}{\partial x^2} - D_{13}\varphi_z\right) = 0$$

The coefficients $A_{ij}, B_{ij}, D_{ij}, C_{ij}, F_{ij}$ and H_{ij} are defined as

$$\{A_{ij}, B_{ij}, D_{ij}, C_{ij}, F_{ij}, H_{ij}\} = \int_{-h/2}^{h/2} Q_{11}\{1, z, z^2, \Phi(z), z\Phi(z), \Phi(z)^2\}dz \, , (i, j = 1,2,6)$$

$$A_{55} = \int_{-h/2}^{h/2} Q_{55}\Phi(z)'^2 dz$$

$$\{A_{13}, B_{13}, C_{13}\} = \int_{-h/2}^{h/2} Q_{13}\{\Phi(z)'', z\Phi(z)'', \Phi(z)\Phi(z)''\}dz \qquad (21)$$

$$D_{33} = \int_{-h/2}^{h/2} Q_{33}\Phi(z)''^2 dz$$

6. Solutions method

This section presents an analytical approach to the equilibrium equations for the FGM nanobeam with simply supported or hinged-hinged (SS) and clamped-clamped (CC) boundary conditions, with the displacement field satisfying these conditions expressed as:

$$\{u_0, \varphi_x\} = \sum_{m=1}^{\infty}\{U_m, \psi_{xm}\}\frac{\partial X_m}{\partial x}$$

$$\{w_0, \varphi_z\} = \sum_{m=1}^{\infty}\{W_m, \psi_{zm}\}X_m \qquad (22)$$

Here, U_m, W_m, ψ_{xm} and ψ_{zm} are arbitrary parameters. The function $X_m(x)$ that satisfy the different boundary conditions are given as

- For Simply supported beam (SS)

$$X_m = \sin(\beta x), \beta = \frac{m\pi}{L} \qquad (23)$$

- For Clamped-Clamped beam (CC)

$$X_m = 1 - \cos(\beta x), \beta = \frac{2m\pi}{L} \qquad (24)$$

By substituting Eqs. (22) in Eq. (20);

$$\begin{bmatrix} K_{11} & K_{12} & K_{13} & K_{14} \\ K_{21} & K_{22} & K_{23} & K_{24} \\ K_{31} & K_{32} & K_{33} & K_{34} \\ K_{41} & K_{42} & K_{43} & K_{44} \end{bmatrix}\begin{Bmatrix} U_m \\ W_m \\ \psi_{xm} \\ \psi_{zm} \end{Bmatrix} = 0 \qquad (25)$$

Stiffness matrix [K] elements are presented in Appendix A.

7. Results and discussion

An FGM beam composed of a mixture of metal and ceramic, specifically an Aluminum alloy (Al) and Alumina (Al₂O₃), is analyzed under various boundary conditions. The material properties are as follows: for Aluminum, Young's modulus $E_m = 70$GPa, and for Alumina $E_c = 380$GPa. The Poisson's ratio is constant at $v = 0.3$.

$$\bar{N} = \frac{N_x^0}{A_{110}}, \quad K_w = \frac{k_w L^2}{A_{110}}, \quad K_g = \frac{k_g}{A_{110}} \tag{26}$$

Where the coefficient A_{110} is of beam made of metal material.

7.1. Comparative study

As an initial example, the results for FG beams derived from the present theory are compared with those obtained using the higher-order shear deformation theory (2D-HSDT) and quasi-3D higher-order beam theory by Vo et al. (2014), Vo et al. (2015). The comparisons are summarized in Table 1 for FG beams with different configurations. A strong agreement between the present results and previous solutions is evident.

Table 1

Comparison of Dimensionless Critical Buckling of FGM Beams

L/h	p	Vo et al. (2014) (2D)	Present (2D)	Error (%)	Vo et al. (2015) (3D)	Present (3D)	Error (%)
		CC					
	0	154.55	152.1476	1.55	160.107	161.9546	1.15
	0.5	103.749	102.2679	1.43	107.655	109.1413	1.38
	1	80.6087	79.4836	1.40	83.6958	84.9202	1.46
	2	61.7925	60.8785	1.48	64.1227	64.947	1.29
	5	47.7562	46.8872	1.82	49.3856	49.6039	0.44
	10	41.8042	40.9887	1.95	43.1579	43.3212	0.38
5		SS					
	0	48.8401	48.596	0.50	49.5901	49.6677	0.16
	0.5	32.0094	31.8654	0.45	32.5867	32.7142	0.39
	1	24.6911	24.5838	0.43	25.2116	25.3845	0.69
	2	19.1605	19.071	0.47	19.6124	19.7906	0.91
	5	15.74	15.6436	0.61	16.0842	16.1693	0.53
	10	14.1468	14.0513	0.68	14.4116	14.4458	0.24
		CC					
	0	195.361	194.3839	0.50	198.706	207.4437	4.40
	0.5	128.05	127.4616	0.46	130.576	136.3172	4.40
	1	98.749	98.3352	0.42	101.02	105.3848	4.32
	2	76.6677	76.284	0.50	78.5783	81.8435	4.16
10	5	62.9786	62.5742	0.64	64.435	66.8867	3.80
	10	56.5971	56.2051	0.69	57.7339	59.9498	3.84
		SS					
	0	52.3082	52.2379	0.13	52.5361	52.6105	0.14
	0.5	34.0087	33.9662	0.12	34.2724	34.3996	0.37

L/h	p	Vo et al. (2014) (2D)	Present (2D)	Error (%)	Vo et al. (2015) (3D)	Present (3D)	Error (%)
		CC					
	1	26.1727	26.1409	0.12	26.4869	26.6722	0.70
	2	20.3936	20.3663	0.13	20.7164	20.9261	1.01
	5	17.1118	17.0818	0.18	17.358	17.4951	0.79
	10	15.5291	15.4994	0.19	15.6895	15.7579	0.44
		CC					
	0	209.233	208.9516	0.13	210.489	222.8882	5.89
	0.5	136.049	135.8649	0.14	137.316	145.2229	5.76
	1	104.716	104.5636	0.15	106.12	112.0462	5.58
	2	81.6035	81.4652	0.17	82.9975	87.4828	5.40
	5	68.4689	68.3271	0.21	69.5392	73.2461	5.33
	10	62.1282	61.9977	0.21	62.8546	66.2914	5.47
20		SS					
	0	53.2546	53.2365	0.03	53.3075	53.3878	0.15
	0.5	34.5488	34.536	0.04	34.7084	34.84	0.38
	1	26.5718	26.562	0.04	26.8174	27.0089	0.71
	2	20.7275	20.7186	0.04	21.0066	21.2266	1.05
	5	17.4935	17.4843	0.05	17.7048	17.858	0.87
	10	15.9185	15.91	0.05	16.0416	16.1209	0.49

$Note. Error$ (%) $= \left| \left(\bar{N}_{Present} - \bar{N}_{Ref} \right) / \bar{N}_{Ref} \right| \times 100\%$
Source. Data analysis result of the research

7.2. Parametric study

7.2.1. Materials properties effect

The effect of the power index "p" and the porosity coefficient "ξ" on the dimensionless critical buckling load of simply supported FG beams is shown in Table 2 and Figures 3 and 4 for Volume Fraction Distribution (VFD) and the Rule of Mixtures Distribution (RMD). In Figure 3, it is evident that the inclusion of porosity reduces the stiffness of the beam. The maximum critical buckling load values are achieved in the case of a perfect beam, where pores are absent. Among the porous beams, the highest critical buckling loads are associated with linear porosity (Type 1), while the lowest is observed for even porosity.

In Figure 4, the value of $p = 0$ indicates that the beam is composed entirely of ceramic, leading to the highest critical buckling load values due to the superior stiffness of the beam in both RMD and VFD cases. As the index "p" increases, the buckling load decreases significantly within the range $0 \leq p \leq 4$, after which the reduction becomes more gradual.

Table 2

Effect of The Power Index "p" and Porosity Coefficient "ξ" on The Dimensionless Critical Buckling Load (L = 10h, SS, $\mu = \lambda = K_w = K_g = 0$)

ξ	p	VFD				RMD			
		Even	**Uneven**	**Linear (1)**	**Linear (2)**	**Even**	**Uneven**	**Linear (1)**	**Linear (2)**
0	**0**	52.6105	52.6105	52.6105	52.6105	52.6105	52.6105	52.6105	52.6105
	1	26.6722	26.6722	26.6722	26.6722	26.6722	26.6722	26.6722	26.6722
	2	20.9261	20.9261	20.9261	20.9261	20.9261	20.9261	20.9261	20.9261
	5	17.4951	17.4951	17.4951	17.4951	17.4951	17.4951	17.4951	17.4951
	10	15.7579	15.7579	15.7579	15.7579	15.7579	15.7579	15.7579	15.7579
0.05	**0**	51.5375	52.3311	52.0723	52.0723	51.0454	52.2213	51.8252	51.8252
	1	25.4337	26.3161	26.2835	25.8194	24.8290	26.1407	26.1077	25.3883
	2	19.5686	20.5113	20.5520	19.9411	18.8985	20.3046	20.3804	19.4429
	5	16.1269	17.0667	17.1168	16.5033	15.4616	16.8602	16.9486	16.0061
	10	14.4980	15.3770	15.3638	14.8860	13.9009	15.1988	15.1904	14.4560
0.1	**0**	50.4645	52.0515	51.5308	51.5308	49.4813	51.8322	51.0346	51.0346
	1	24.1823	25.9568	25.8940	24.9480	22.9572	25.6030	25.5436	24.0658
	2	18.1811	20.0897	20.1778	18.9243	16.8035	19.6690	19.8361	17.8927
	5	14.7139	16.6272	16.7379	15.4662	13.3219	16.2014	16.4024	14.4165
	10	13.2028	14.9857	14.9676	13.9700	11.9569	14.6165	14.6195	13.0530
0.15	**0**	49.3915	51.7717	50.9859	50.9859	47.9181	51.4432	50.2381	50.2381
	1	22.9163	25.5944	25.5040	24.0570	21.0517	25.0585	24.9798	22.7012
	2	16.7583	19.6608	19.8034	17.8727	14.6240	19.0175	19.2932	16.2674
	5	13.2448	16.1754	16.3583	14.3778	11.0340	15.5147	15.8561	12.7084
	10	11.8610	14.5822	14.5691	13.0034	9.8800	14.0052	14.0440	11.5264
0.2	**0**	48.3186	51.4916	50.4373	50.4373	46.3557	51.0542	49.4353	49.4353
	1	21.6338	25.2286	25.1132	23.1451	19.1058	24.5068	24.4160	21.2906
	2	15.2939	19.2240	19.4288	16.7833	12.3365	18.3485	18.7514	14.5576
	5	11.7039	15.7098	15.9780	13.2313	8.5295	14.7950	15.3093	10.8591
	10	10.4560	14.1646	14.1679	11.9777	7.5849	13.3563	13.4624	9.8461

Source. Data analysis result of the research

Figure 3

Effect of The Porosity Coefficient "ζ" on The Dimensionless Critical Buckling of Simply Supported FG Beam ($p = 2, L = 10h, \mu = \lambda = K_w = K_g = 0$)
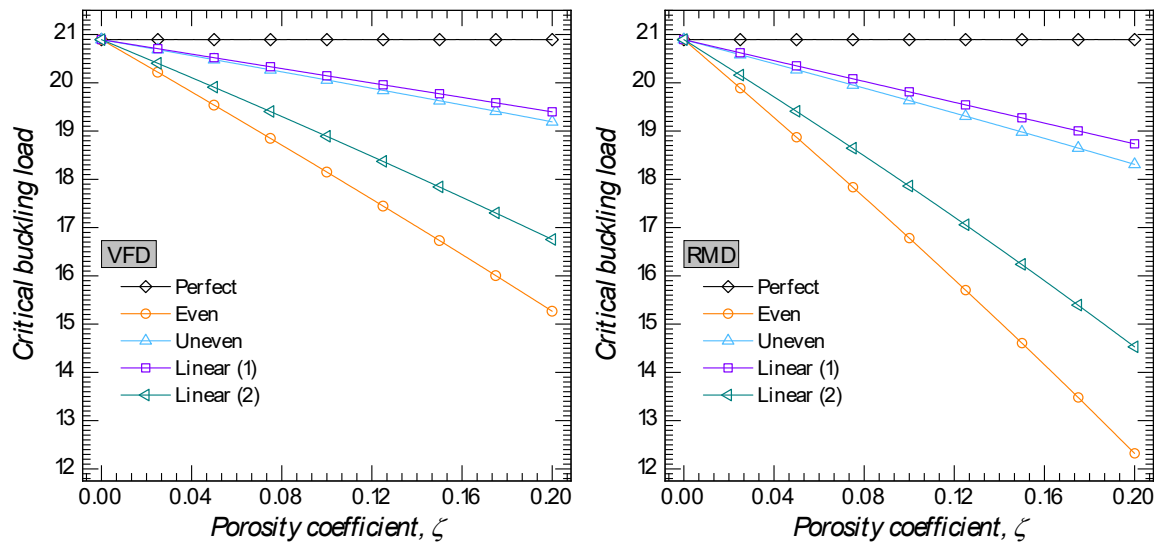
Source. The researcher's data analysis

Figure 4

Effect of The Power Law Index "p" and The Porosity Coefficient "ζ" on The Dimensionless Critical Buckling of Simply Supported FG Beam (L = 10h, μ = λ = K_w = K_g = 0)
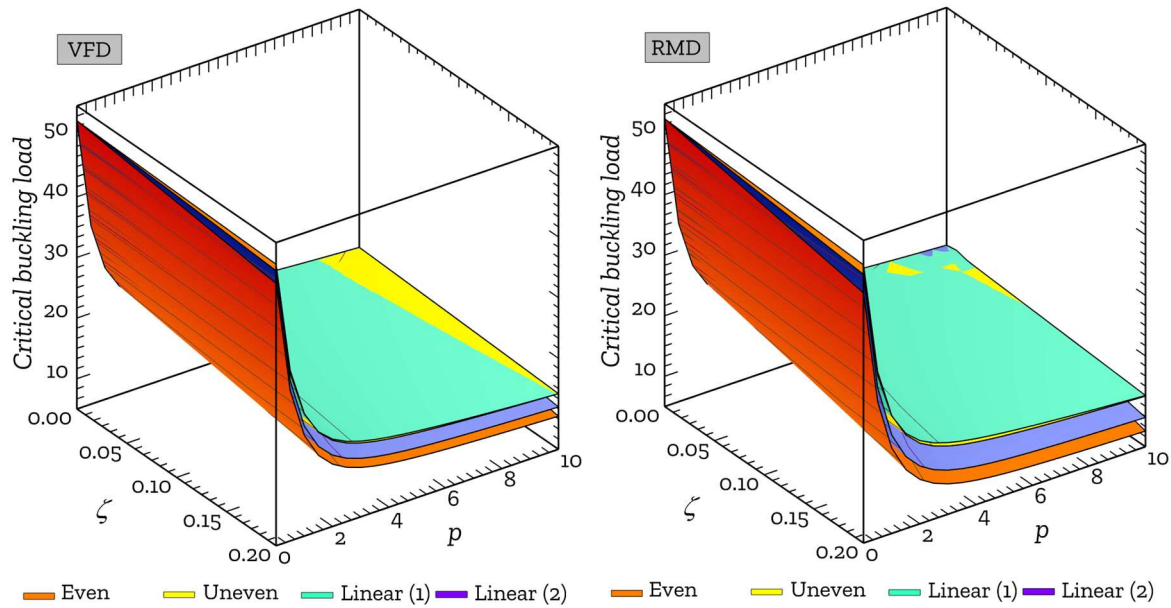
Source. The researcher's data analysis

7.2.2. Beam geometry effect

The effect of the geometric parameter L/h and boundary conditions on the critical buckling load of simply supported FG beams with even porosity is presented in Table 3. The power law index and the porosity coefficient are set at $p = 2$ and $\xi = 0.2$. It is observed that increasing the thickness ratio leads to an increase in the dimensionless critical buckling load.

Table 3

The Effect of The Geometric Parameter "L/h" and Boundary Conditions on The Critical Buckling Load (p = 2, Even, ξ = 0.2, μ = λ = K_w = K_g = 0)

BCs	L/h	VFD				RMD			
		Even	Uneven	Linear (1)	Linear (2)	Even	Uneven	Linear (1)	Linear (2)
SS	5	14.5386	18.1098	18.3438	15.9723	11.7904	17.2831	17.6917	13.9217
	10	15.2939	19.2240	19.4288	16.7833	12.3365	18.3485	18.7514	14.5576
	15	15.4407	19.4431	19.6414	16.9406	12.4420	18.5582	18.9591	14.6803
	20	15.4926	19.5208	19.7167	16.9963	12.4792	18.6326	19.0328	14.7236
	30	15.5298	19.5766	19.7707	17.0362	12.5060	18.6860	19.0856	14.7547
CC	5	48.5015	58.7381	59.8892	53.4711	39.8580	55.9777	57.4295	47.2735
	10	59.8554	74.7629	75.8784	65.7669	47.8632	71.0541	72.5384	56.9402
	15	62.5462	78.7140	79.7916	68.6674	49.6958	74.7600	76.2192	59.1619
	20	63.5443	80.1953	81.2557	69.7420	50.3696	76.1482	77.5947	59.9795
	30	64.2764	81.2872	82.3340	70.5298	50.8617	77.1711	78.6071	60.5770
CF	5	4.1674	5.2876	5.3758	4.5747	3.2340	4.9897	5.0706	3.8922
	10	4.2471	5.4068	5.4957	4.6607	3.2840	5.0990	5.1791	3.9555
	15	4.2622	5.4295	5.5185	4.6770	3.2935	5.1199	5.1997	3.9675
	20	4.2675	5.4375	5.5266	4.6827	3.2968	5.1272	5.2070	3.9717
	30	4.2713	5.4432	5.5323	4.6869	3.2992	5.1324	5.2122	3.9747

7.2.3. Small scale effect

Table 4 and Figure 5 demonstrate the effects of the nonlocal parameter "μ" and the length-scale parameter "λ" on the dimensionless critical buckling load of FG beams. It is noted that as the nonlocal parameter "μ" increases, the dimensionless critical buckling load decreases, suggesting that the nonlocal effect induces a stiffness-softening behavior. In contrast, an increase in the length-scale parameter "λ" results in a rise in the dimensionless critical buckling load.

Table 4

Effect of the Nonlocal Parameter "μ" and Length Scale Parameter "λ" on The Dimensionless Critical Buckling Load ($p = 2, \xi = 0.2, L = 10h, SS, K_w = K_g = 0$)

μ	λ	VFD				RMD			
		Even	Uneven	Linear (1)	Linear (2)	Even	Uneven	Linear (1)	Linear (2)
0	0	15.2939	19.2240	19.4288	16.7833	12.3365	18.3485	18.7514	14.5576
	0.5	16.0408	20.1645	20.3813	17.6032	12.9378	19.2454	19.6710	15.2675
	1	16.7878	21.1050	21.3337	18.4232	13.5391	20.1424	20.5905	15.9773
	1.5	17.5348	22.0456	22.2862	19.2432	14.1404	21.0393	21.5101	16.6871
	2	18.2818	22.9861	23.2386	20.0632	14.7418	21.9362	22.4297	17.3970
0.5	0	14.5746	18.3199	18.5151	15.9940	11.7564	17.4856	17.8696	13.8730
	0.5	15.2865	19.2162	19.4228	16.7754	12.3294	18.3404	18.7459	14.5495
	1	15.9984	20.1125	20.3304	17.5568	12.9024	19.1951	19.6222	15.2259
	1.5	16.7102	21.0088	21.2381	18.3382	13.4755	20.0499	20.4985	15.9024
	2	17.4221	21.9052	22.1458	19.1196	14.0485	20.9046	21.3749	16.5788
1	0	13.9200	17.4971	17.6835	15.2756	11.2283	16.7003	17.0669	13.2499
	0.5	14.5999	18.3531	18.5504	16.0219	11.7756	17.5166	17.9039	13.8960
	1	15.2798	19.2092	19.4173	16.7682	12.3229	18.3330	18.7409	14.5420
	1.5	15.9597	20.0652	20.2842	17.5146	12.8702	19.1493	19.5779	15.1881
	2	16.6396	20.9213	21.1511	18.2609	13.4175	19.9657	20.4148	15.8342
1.5	0	13.3217	16.7450	16.9234	14.6190	10.7457	15.9824	16.3333	12.6804
	0.5	13.9723	17.5642	17.7530	15.3332	11.2694	16.7637	17.1343	13.2987
	1	14.6230	18.3835	18.5827	16.0475	11.7932	17.5449	17.9353	13.9170
	1.5	15.2737	19.2027	19.4123	16.7617	12.3170	18.3262	18.7363	14.5353
	2	15.9243	20.0220	20.2419	17.4759	12.8408	19.1075	19.5373	15.1536
2	0	12.7726	16.0549	16.2259	14.0165	10.3028	15.3237	15.6602	12.1578
	0.5	13.3965	16.8404	17.0214	14.7013	10.8050	16.0728	16.4282	12.7506
	1	14.0203	17.6258	17.8168	15.3861	11.3072	16.8219	17.1961	13.3434
	1.5	14.6442	18.4113	18.6122	16.0709	11.8094	17.5709	17.9641	13.9362
	2	15.2680	19.1968	19.4077	16.7557	12.3116	18.3200	18.7321	14.5290

Figure 5

Effect of The Nonlocal Parameter "μ" and The Length Scale Parameter "λ" on The Dimensionless Critical Buckling of Simply Supported FG Beam ($p = 2, Even, \zeta = 0.2, L = 10h, K_w = K_g = 0$)
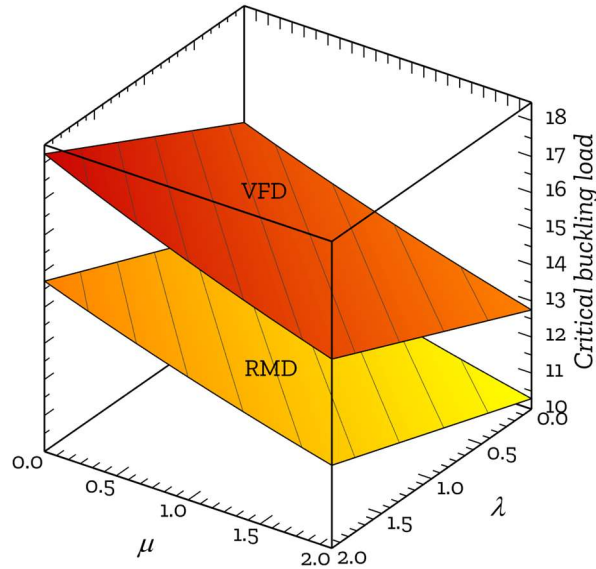
7.2.4. Winker/Pasternak elastic foundation effect

Table 5 and Figure 6 illustrates the dimensionless critical buckling load of FG beams influenced by Winkler/Pasternak elastic foundations. The inclusion of the foundation enhances the rigidity of the beams, with increases in the parameters "K_w" and "K_g" leading to higher values of the dimensionless critical buckling load.

Table 5

The Effect of The Elastic Foundation Parameters "K_w" and "K_g" on The Critical Buckling Load ($p = 2, \xi = 0.2, SS, \mu = \lambda = 0$)

$K_w(\times 10^{-2})$	$K_g(\times 10^{-2})$	VFD				RMD			
		Even	**Uneven**	**Linear**	**Linear**	**Even**	**Uneven**	**Linear**	**Linear**
0	**0.0**	15.2940	19.2241	19.4290	16.7834	12.3366	18.3487	18.7514	14.5576
	0.2	17.6940	21.6241	21.8290	19.1834	14.7366	20.7487	21.1514	16.9576
	005	21.2940	25.2241	25.4290	22.7834	18.3366	24.3487	24.7514	20.5576
	008	24.8940	28.8241	29.0290	26.3834	21.9366	27.9487	28.3514	24.1576
	1.0	27.2940	31.2241	31.4290	28.7834	24.3366	30.3487	30.7514	26.5576
2	**0.0**	17.7257	21.6558	21.8607	19.2151	14.7683	20.7804	21.1831	16.9893
	0.2	20.1257	24.0558	24.2607	21.6151	17.1683	23.1804	23.5831	19.3893
	0.5	23.7257	27.6558	27.8607	25.2151	20.7683	26.7804	27.1831	22.9893
	0,8	27.3257	31.2558	31.4607	28.8151	24.3683	30.3804	30.7831	26.5893
	1.0	29.7257	33.6558	33.8607	31.2151	26.7683	32.7804	33.1831	28.9893
5	**0.0**	21.3732	25.3034	25.5082	22.8627	18.4158	24.4280	24.8307	20.6369
	0.2	23.7732	27.7034	27.9082	25.2627	20.8158	26.8280	27.2307	23.0369
	0.5	27.3732	31.3034	31.5082	28.8627	24.4158	30.4280	30.8307	26.6369
	0.8	30.9732	34.9034	35.1082	32.4627	28.0158	34.0280	34.4307	30.2369
	1.0	33.3732	37.3034	37.5082	34.8627	30.4158	36.4280	36.8307	32.6369
8	**0.0**	25.0208	28.9510	29.1558	26.5102	22.0634	28.0755	28.4782	24.2845
	0.2	27.4208	31.3510	31.5558	28.9102	24.4634	30.4755	30.8782	26.6845
	0.5	31.0208	34.9510	35.1558	32.5102	28.0634	34.0755	34.4782	30.2845
	0.8	34.6208	38.5510	38.7558	36.1102	31.6634	37.6755	38.0782	33.8845
	1.0	37.0208	40.9510	41.1558	38.5102	34.0634	40.0755	40.4782	36.2845

$K_w(\times 10^{-2})$	$K_g(\times 10^{-2})$	VFD				RMD			
		Even	Uneven	Linear	Linear	Even	Uneven	Linear	Linear
10	**0.0**	27.4525	31.3827	31.5875	28.9419	24.4951	30.5072	30.9100	26.7162
	0.2	29.8525	33.7827	33.9875	31.3419	26.8951	32.9072	33.3100	29.1162
	0.5	33.4525	37.3827	37.5875	34.9419	30.4951	36.5072	36.9100	32.7162
	0.8	37.0525	40.9827	41.1875	38.5419	34.0951	40.1072	40.5100	36.3162
	1.0	39.4525	43.3827	43.5875	40.9419	36.4951	42.5072	42.9100	38.7162

Source. Data analysis result of the research

Figure 6

Effect of Winkler Foundation Parameter "K_w" and Pasternak Foundation Parameter "K_g" on The Dimensionless Critical Buckling of Simply Supported FG Beam ($p = 2, L = 10h, \zeta = 0.2, \mu = \lambda = 0$)
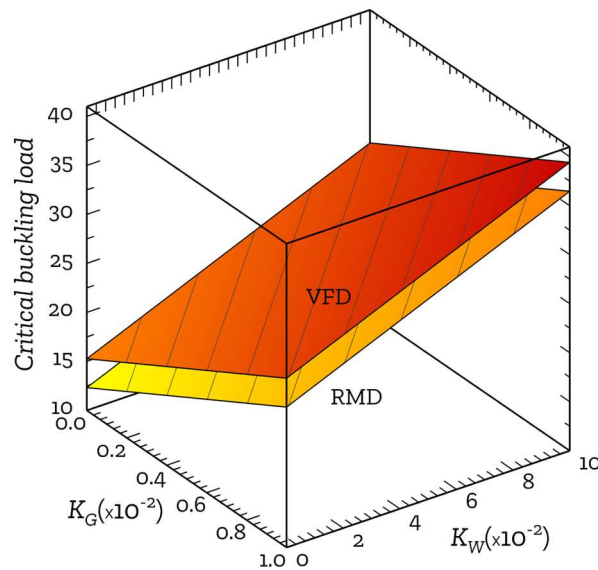
Source. The researcher's data analysis

8. Conclusion

In conclusion, this study provides a comprehensive analysis of the impact of porosity on the buckling behavior of functionally graded beams. By integrating two distinct porosity schemes - volume fraction-dependent and rule of mixtures-dependent - we established a novel framework that clarifies the relationship between porosity and material volume fraction.

The analysis demonstrates that increases in the porosity coefficient result in significant reductions in critical buckling loads, regardless of the type of porosity distribution. Furthermore, we investigated the effects of geometric parameters, nonlocal influences, and foundation stiffness on the overall structural rigidity and stability.

The proposed technique is currently limited to simple beams with uniform thickness, straight geometries, and specific boundary conditions, namely simply supported and clamped configurations.

Overall, this work enhances the understanding of how porosity and material distribution affect the mechanical performance of functionally graded beams, offering valuable insights for the design and optimization of advanced materials in engineering applications. Future research could focus on experimental validation of the proposed models and the exploration of various material combinations and loading conditions.

References

Adhikari, B., Dash, P., & Singh, B. (2020). Buckling analysis of porous FGM sandwich plates under various types of non-uniform edge compression based on higher order shear deformation theory. *Composite Structures, 251*, Article 112597.

Akbaş, S. D. (2017). Nonlinear static analysis of functionally graded porous beams under thermal effect. *Coupled Systems Mechanics, 6*(4), 399-415.

Anirudh, B., Ganapathi, M., Anant, C., & Polit, O. (2019). A comprehensive analysis of porous graphene-reinforced curved beams by finite element approach using higher-order structural theory: bending, vibration and buckling. *Composite Structures, 222*, Article 110899.

Atmane, H. A., Tounsi, A., & Bernard, F. (2017). Effect of thickness stretching and porosity on mechanical response of a functionally graded beams resting on elastic foundations. *International Journal of Mechanical Materials Design, 13*, 71-84.

Bagheri, Z., Fiouz, A., & Seraji, M. (2024). Effect of porosity on free vibration and buckling of functionally graded porous beams with non-uniform cross-section. *Journal of Central South University, 31*(3), 841-857.

Beitollahi, A., Bazargan-Lari, Y., & Janghorban, M. (2024). On the variable length scale parameter in functionally graded non-porous and porous microplate/nanoplate. *Mechanics of Advanced Materials and Structures, *(30), 12481-12503.

Burlayenko, V. N., & Kouhia, R. (2024). Analysis of natural frequencies in non-uniform cross-section functionally graded porous beams. *Journal of Vibration Engineering and Technologies, 12*, 6527-6547.

Chen, D., Kitipornchai, S., & Yang, J. (2016). Nonlinear free vibration of shear deformable sandwich beams with a functionally graded porous core. *Thin-Walled Structures, 107*, 39-48.

Chen, D., Yang, J., & Kitipornchai, S. (2015). Elastic buckling and static bending of shear deformable functionally graded porous beams. *Composite Structures, 133,* 54-61.

Eltaher, M. A., Fouda, N., El-Midany, T., & Sadoun, A. M. (2018). Modified porosity model in analysis of functionally graded porous nanobeams. *Journal of the Brazilian Society of Mechanical Sciences and Engineering, 40*(3).

Fahsi, B., Bouiadjra, R. B., Mahmoudi, A., Benyoucef, S., & Tounsi, A. (2019). Assessing the effects of porosity on the bending, buckling, and vibrations of functionally graded beams resting on an elastic foundation by using a new refined quasi-3D theory. *Mechanics of Composite Materials, 55*(2), 219-230.

Fallah, A., & Aghdam, M. M. (2024). Physics-informed neural network for bending and free vibration analysis of three-dimensional functionally graded porous beams resting on elastic foundation. *Engineering Computations, 40*(1), 437-454.

Gao, Y., & Xiao, W. (2019). Nonlinear bending of functionally graded porous nanobeam subjected to multiple physical loads based on nonlocal strain gradient theory. *Steel and Composite Structures, 31*(5), 469-488.

Hamed, M., Abo-Bakr, R., Mohamed, S., & Eltaher, M. (2020). Influence of axial load function and optimization on static stability of sandwich functionally graded beams with porous core.

Engineering Computations, 36(4), 1929-1946.

Hamed, M., Sadoun, A., & Eltaher, M. A. (2019). Effects of porosity models on static behavior of size dependent functionally graded beams. *Structural Engineering and Mechanics, 71*(1), 89-98.

Li, S.-R., & Batra, R. C. (2013). Relations between buckling loads of functionally graded Timoshenko and homogeneous Euler-Bernoulli beams. *Composite Structures, 95*, 5-9.

Liu, Y., Su, S., Huang, H., & Liang, Y. (2019). Thermal-mechanical coupling buckling analysis of porous functionally graded sandwich beams based on physical neutral plane. *Composites Part B: Engineering, 168*, 236-242.

Masjedi, P. K., Maheri, A., & Weaver, P. M. (2019). Large deflection of functionally graded porous beams based on a geometrically exact theory with a fully intrinsic formulation. *Applied Mathematical Modelling, 76*, 938-957.

Mellal, F., Bennai, R., Nebab, M., Atmane, H. A., Bourada, F., Hussain, M., & Tounsi, A. (2021). Investigation on the effect of porosity on wave propagation in FGM plates resting on elastic foundations via a quasi-3D HSDT. *Waves in Random and Complex Media, 30*(13), 2765-2779.

Mojahedin, A., Jabbari, M., & Rabczuk, T. (2018). Thermoelastic analysis of functionally graded porous beams. *Journal of Thermal Stresses, 41*(8), 937-950.

Nebab, M., Dahmane, M., Belqassim, A., Atmane, H. A., Bernard, F., Benadouda, M., Bennai, R., & Hadji, L. (2023). Fundamental frequencies of cracked FGM beams with influence of porosity and Winkler/Pasternak/Kerr foundation support using a new quasi-3D HSDT. *Mechanics of Advanced Materials and Structures, 31*(28), 10639-10651.

Polit, O., Anant, C., Anirudh, B., & Ganapathi, M. (2019). Functionally graded graphene reinforced porous nanocomposite curved beams: bending and elastic stability using a higher-order model with thickness stretch effect. *Composites Part B: Engineering, 166*, 310-327.

Sah, S. K., & Ghosh, A. (2022). Influence of porosity distribution on free vibration and buckling analysis of multi-directional functionally graded sandwich plates. *Composite Structures, 279*, Article 114795.

Srikarun, B., Songsuwan, W., & Wattanasakulpong, N. (2021). Linear and nonlinear static bending of sandwich beams with functionally graded porous core under different distributed loads. *Composite Structures, 276*, Article 114538.

Su, J., Xiang, Y., Ke, L.-L., & Wang, Y.-S. (2019). Surface effect on static bending of functionally graded porous nanobeams based on Reddy's beam theory. *International Journal of Structural Stability and Dynamics, 19*(6), Article 1950062.

Truong, C. H., Tran, T. M., Do, D. M., & Tran, H. Q. (2021). Static flexural analysis of sandwich beam with functionally graded face sheets and porous core via point interpolation meshfree method based on polynomial basic function. *Archives of Applied Mechanics, 91*(3), 933-947.

Vo, T. P., Thai, T. H., Nguyen, K. T., Inam, F., & Lee, J. (2015). A quasi-3D theory for vibration and buckling of functionally graded sandwich beams. *Composite Structures, 119*, 1-12.

Vo, T. P., Thai, T. H., Nguyen, K. T., Maheri, A., & Lee, J. (2014). Finite element model for vibration and buckling of functionally graded sandwich beams based on a refined shear deformation theory. *Engineering Structures, 64*, 12-22.

Wang, Y., Zhou, A., Fu, T., & Zhang, W. (2020). Transient response of a sandwich beam with functionally graded porous core traversed by a non-uniformly distributed moving mass. *International Journal of Mechanical Materials Design, 16*(3), 519-540.

Wattanasakulpong, N., & Ungbhakorn, V. (2014). A study on functionally graded materials. *Aerospace Science and Technology, 32*, Article 111.

Zghal, S., & Dammak, F. (2021). Buckling responses of porous structural components with gradient power-based and sigmoid material variations under different types of compression loads. *Composite Structures, 273*, Article 114313.

Zghal, S., Ataoui, D., & Dammak, F. (2020). Static bending analysis of beams made of functionally graded porous materials. *Mechanics Based Design of Structures and Machines, 50*(3), 1-18.

Zhang, X., Wang, H., Zheng, S., & Chen, D. (2024). Size-dependent nonlinear free vibration of multilayer functionally graded graphene platelet-reinforced composite tapered microbeams. *Journal of Vibration Engineering and Technologies, 12*, 7653-7670.

Zhang, Y., Jin, G., Chen, M., Ye, T., Yang, C., & Yin, Y. (2020). Free vibration and damping analysis of porous functionally graded sandwich plates with a viscoelastic core. *Composite Structures, 244*, Article 112298.

Zouatnia, N., Hadji, L., Atmane, H. A., Nebab, M., Madan, R., Bennai, R., & Dahmane, M. (2024). Analysis of free vibration in bi-directional power law-based FG beams employing RSD theory. *Coupled Systems Mechanics, 13*(4), Article 359.